Soft-sensing reconstruction of in-depth defect geometry from active IR-thermography data

Soft-sensing reconstruction of in-depth defect geometry from active IR-thermography data

P. Castellini, M. Martarelli, A. D'Antuono, N. Paone

Department of Industrial Engineering and Mathematical Sciences, Università Politecnica delle Marche, Ancona, Italy

E-mail: m.martarelli@staff.univpm.it

Received xxxxxx
Accepted for publication xxxxxx
Published xxxxxx

Abstract

This paper proposes a new approach for processing measured data from active IR (Infra Red) thermography, where a soft sensing algorithm is exploited for in depth defect reconstruction. This is achieved by propagating the information gathered at the wall surface to the inner layers. Correlating the experimental 2D measurements to a Finite Element (FE) model of the tested specimen it is possible to update the model with the measured data and change the geometry of the simulated inner defect, until the surface temperature distribution calculated corresponds to the measured one. Following that strategy, the unknown defect geometry can be determined. The method developed and presented in this paper consists of an optimization problem based on the minimization of the difference between the surface temperature distribution measured on the sample subjected to an active thermography test and the one resulting from the FE model. The optimization variables are the geometrical parameters (depth, width, thickness and position) characterizing the defect which will be fully determined at the complete convergence, within a given tolerance, of the optimization problem. The method includes also a preprocessing algorithm, based on the same experimental data and FE model, which allows to determine thermal and mechanical properties of the object under test, like surface emissivity, heat capacity and material conductivity and density, which are often unknown especially in the case of works of art. This soft-sensing procedure has been applied to a virtual experiment to estimate the accuracy of the reconstructed geometry and to a simulacrum of ancient fresco including defects realized on purpose.

Keywords: Active Thermography; Defect shape reconstruction; Soft-sensing; Non-Destructive Testing; Defect Diagnostics

1. Introduction

Active Infra-Red (IR) thermography ([1], [2]) is a well-established Non-Destructive Testing technique for the detection of thermal discontinuities, which are in general associated to damage or defects hidden under the surface (for example delamination and layer detachment). Thanks to its ability to monitor the structural integrity of complex structures, it has been applied to different classes of materials exploited in various sectors, from aerospace ([3], [4]), and specifically for composite material integrity investigation ([5], [6] in the latter the joint application of thermography and 3D laser scanner allowed 3D inspections), to the cultural heritage ([7], [8]). Peculiar implementations of active thermography are the Lock-In Thermography (LIT, [9], [10], [11]) the Pulsed-Thermography (PT, [12], [13]) which are based on the observation of the surface temperature response of the item under test produced by the heat conduction across the stratigraphy of the component itself which a periodic

modulated, for LIT, or a transient, specifically a pulse for PT, thermal load is imposed to. PT exhibits the advantages of being non-contact due to the optical nature of IR imaging systems and a very fast measurement technique due to the short duration of the pulse and of the following thermal transient. In practice the acquisition duration depends on the thermal pulse propagation across the component which can ranges from few milliseconds for metals (high conductive materials) to some seconds for composites and building elements (made of concrete, bricks or wood). Commonly used pulse thermal radiators are in the visible range (e.g. halogen lamps) but also infrared emitters or lasers.

The analysis of the surface temperature of the loaded element by means of IR thermography allows detecting inhomogeneities in the stratigraphy because the surface temperature decays as long as the heat can flow off into the interior, depending on local thermal diffusivity. If an air inclusion is present due to a delamination the heat is trapped into the air cushion and the temperature cannot further decrease. PT allows therefore to evaluate the extension of the inclusion by only observing the thermograms giving a qualitative estimation of the defect geometry. By applying advanced signal processing to the thermal images sequence acquired during the thermal load propagation across the element under test, geometrical characteristics of the potential defect can also be quantified. Among the many examples, it is worth mentioning [14] where the authors succeed in improving the probing depth of the thermographic detection. Recently, Liu et al., in [15] and [16], have proposed the application of Principal Component Analysis (PCA) and Generative PCA for quality assessment of polymeric composites. A Spatial-Neighborhood Manifold Learning algorithm has been applied in [17] for defect localization in carbon fiber-reinforced polymer (CFRP). In [18] Theodorakeas et al. presented a defect depth retrieval method based on two possible approaches: either the analysis of the temperature-contrast time first-derivative variation or the evaluation of the phase-contrast variation in the frequency domain. Such procedure is part of the empirical methods category which evaluate the contrast between sound and damaged areas. If defects are spread all over the area under test and framed by the Infra-Red camera and therefore any region of the thermogram can be assumed as a sound area, it is possible to resort to the second derivative of the temperature contrast which is unfortunately a very noisy function due to the derivative operation and makes the method less accurate.

To overcome the limits of empirical procedures, analytical (1D thermal diffusion equation) and numerical models (Finite Element Methods, FEM and Finite Difference Methods, FDM) have been applied to make the quantification of discontinuities in the geometry from the thermal maps more accurate. Simplified mono-dimensional models have been used for the detachment modelling and for grounding their recognition and localization on a correlation between experimental thermograms and modelled ones ([19]). In [20] Lugin et al.a proposed a model to estimate the thickness of samples that have rear faces partially or completely inaccessible: the model is exploited in conjunction with experimental data obtained via PT in order to estimate the depth of the defect. In practice a guess of the defect depth is retrieved from the IR thermogram sequence by applying the so-called echo defect shape (EDS) algorithm. This method takes into account that the reflection of the thermal wave in the defect interface, when returning towards the wall top surface, produces an increase of the temperature in the surface itself and that the time evolution of this temperature can be fitted by an exponential curve. The depth estimated by the model is therefore corrected with the guess value in a certain number of iterations until the guess value and the calculated one are equal with a defined tolerance. The method has been improved in [21] and [22] by taking into account the effect of the opening angle in the reconstruction of the defect, considering the case of a triangular geometry. Further examples of defect morphology (extension and depths) estimation methods based on the coupling of PT experiments and FEM/FDM models and applied to architectonic structures' health assessment have been presented in the works [23], [24].

To avoid the iteration process and speed up the defect depth retrieval procedure, it has been proposed to use the 1D analytical model as interpolant curve of the IR thermogram sequence adopting a Nonlinear System Identification (NSI) strategy [25]. This method allows to estimate the defect depth in a more automatic and flexible manner but presents the limitation of being a data-driven method considering an ideal heat diffusion model and not the specific one realized in the inspection process.

To automate the iteration process, some researchers have proposed to use Finite Element models in an optimization loop to solve the inverse heat transfer problem. Marcuzzi, in [26], has implemented an adaptive FEM into a predictor-corrector algorithm to reconstruct corrosion profiles starting from IR thermograms. Richter, in [27], has applied an optimization method based on FEM and IR data for the reconstruction of back-wall geometry, i.e. the defects are represented as open inclusions producing discontinuities on the inaccessible surface of the element under test.

In this paper we present a further step of FEM based iterative procedures consisting of an optimization algorithm for the reconstruction of the real stratigraphy of elements under test including internal defects of arbitrary shapes. The use of models as part of the measurement process is indeed a form of soft-sensing [28], [29]. The model has been exploited for both generating synthetized data emulating an IR thermal map (thermogram) produced by the heat flow within an unknown geometry and reconstructing the correct stratigraphy of the element under test by using the synthetized data. Those synthetized data allowed to reproduce a virtual experiment described in Section 2.2 and used to validate the algorithm proposed (Section 4.1).

The defect reconstruction method described in this work presents the following advances with respect to the state-of-the-art of soft sensors based on FE methods:

- the optimization algorithm is suitable for inner defects of arbitrary shape, not only triangular defects and back-wall open inclusions
- the FE model exploited in the optimization considers realistic heat flow distribution by taking into account the emissivity of the surface facing to the heat source and the mechanical and thermal characteristics of the material recovered from the measured thermograms
- the optimization algorithm uses an arbitrary initial guess of the defect depth based on the measured temperature time history and not the EDS.

The application of the method to a real structure (illustrated in Section 2.3) is reported in Section 4.3. The structure is a simulacrum of an ancient fresco hosting in-depth defects realized on purpose. The non-invasive and non-destructive detection of hidden damage in frescoes paintings has attracted the interest of researchers since the 90s. Several measurement methods have been developed for the diagnosis of hidden defects such as detachments between plaster and supporting wall, or between plaster layers and paint layer, as well as cracks; these damages generally originate below the surface and should be detected before they grow and reach the pictorial surface or compromise local stability of the fresco. Non-contact methods operated from a distance should be preferred, due to the delicate nature of ancient frescoes paintings and to the fact that they are often located on walls not easy to be accessed in proximity. Vibration based diagnosis gathered large interest and proved very effective to detect detachments and delaminations in works of art; in particular, laser scanning vibrometry under acoustic excitation was successfully demonstrated both in laboratory conditions and on real frescoes [30], [31], [32], [33]. Despite this successful series of demonstrations, laser vibrometry still requires specific skill in vibration testing, which is not common in professionals working in restoration of artworks, and requires long acquisition time, being a technique, which implies the sequential scanning of hundreds of points on the surface of the artwork. Full field optical techniques for deformation measurement have been developed as an alternative and demonstrated on various types of works of art, which exhibit internal defects in the form of delaminations. In particular interferometric techniques [34], among which holographic interferometry [35][34], electronic speckle interferometry ([36] and [37]), shearography and tera-hertz imaging [38] have been successfully demonstrated for structural damage assessment on several types of artworks; however, their application to large surfaces is still challenging and, again, they require skilled operators with expertise on the specific measurement technique. Acoustic based diagnostics is a further contactless method which has been applied to structural damage identification in paintings, the acoustic energy absorption coefficient of the panel tested being correlated to its stratigraphy [39]. Among the optical techniques which can be applied to large surfaces, Active IR thermography is attracting a growing interest, because its operating principle is intrinsically simpler than interferometric techniques, and its application to large surfaces such as frescoes paintings is relatively simpler, [40].

2. Material and methods

2.1 Active IR thermography

Active IR thermography is based on the measurement of the 2D thermal emission of an object surface when the object is exposed to a thermal flux. The thermal flux propagation inside the object affects its surface temperature; therefore, depending also on local emissivity, the infrared emission from the surface varies, which can be measured by an IR thermal camera as an image. The presence of defects inside the object, as detachment between different layers, modifies the propagation of the heat flow and consequently the surface temperature distribution, which can be used for the damage identification. This concept is illustrated in Figure 1: the pulsed thermal load W(t) (black signal on the top left side of the scheme) generated by the flash lamps impinges to the surface of the object under test and is framed by the IR camera (IR Cam) which register time histories of the surface infrared emission at any pixel of its field of view. Indeed, for given surface emissivity, the increase in infrared emission correlates to an increase in surface temperature; if local emissivity is known, this correlation allows to measure surface temperature distribution. As an example, the time history T(t) registered on a pixel located in a healthy region will have the trend of the green signal on the top right side of the scheme while the one registered on region presenting a defect will have the trend of the red signal T(t) on the bottom right side. Due to the reflection of the thermal wave by the defect surface, the temperature on the object surface and the following infrared emission will undergo an evident increment.

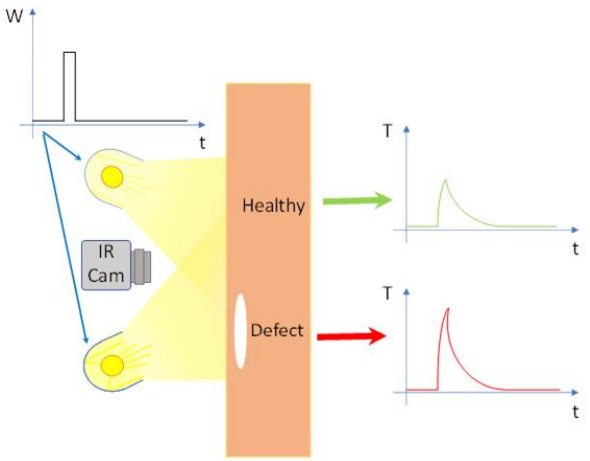

Figure 1 Active IR thermography concept

Performance of this technique strongly depends on the thermal characteristics of the structure under test (stratigraphy, hence thermal diffusivity, and surface emissivity) which are obviously independent parameters out of control of the experimentalist. In order to improve the accuracy of the measurement the experimental parameters that can be optimized are the ones related to the heating source, like power W and heating duration. Such optimization must take into account the fact that the thermal distribution on the surface framed by the IR camera will be affected by internal voids (or layer discontinuities) with a limitation: increasing the defect depth its effect on the surface thermal distribution fades away up to be buried into the measurement noise. This fading effect is enhanced by the stratigraphy thermal conductivity, which is not necessarily isotropic, but certainly not 1D, e.g. the propagation direction cannot realistically be considered purely orthogonal to the framed surface. The awareness of this effect drives the choice of the experimental parameters but is usually not taken into account in the post-processing of thermography map sequences, which are commonly visually observed or parametrized to extract defect features by correlating them with 1D propagation models.

In this paper a 2D propagation model is set to consider the fading effect in a realistic way. The model will be used in conjunction with experimental thermograms acquired during an active thermography test to reconstruct the defect shape and depth by exploiting an optimization procedure. Since such procedure makes use of both numerical (software based) and experimental (sensor based) data it is so-called soft-sensing. Being aware that the most critical aspect of soft-sensing optimization methods is the knowledge of model parameters (material conductivity and density, infrared illumination intensity and distribution and surface emissivity, which altogether determine thermal load) specific procedures for experimentally assess those parameters is also defined and tested.

The soft-sensing reconstruction method has been first tested and validated on synthetized data obtained by running the 2D model used for the soft-sensing reconstruction itself and finally verified on a real structure described in the following sub-sections.

2.2 2D FE model

A 2D FE model has been set to replicate a sort of virtual experiment, that allowed to synthetize thermal distribution time sequences on the modeled object surface as they could be measured by an IR camera framing the surface of the real object subjected to a thermal load. The FE model has been realised in Matlab using the Partial Differential Equation Toolbox.

The modeled geometry is a rectangle representing a cross section of a building element of width 1 m and thickness of 0.1 m made of concrete. The element presents an elliptical defect of 200x15 mm size placed at 2.5 mm from the surface facing the heating source and that would be framed by an IR camera in a real experiment. Figure 2 (a) shows a close-up of the modeled geometry around the damaged region and Figure 2 (b) the mapped structured mesh on the same region.

For each iteration the geometry of the defect is not unknown: it is given as a hypothesis which will converge to the optimal value at the end of iteration. The defect shape needs to be defined a priori from a predefined set of shapes, i.e. rectangular, elliptical and/or polynomial geometry, depending on available a-priori information and operator choices. The current position and shape of the defect is modified at each iteration, by changing the polynomial coefficients, in the case of polynomial geometry. At each iteration a mapped structured mesh of triangular elements is regenerated automatically.

The model physics is the heat transmission and the initial condition is uniform temperature of 293.15 K for air and solid. The boundary load condition on the right side of the sample as in Figure 2 (a) is the heating of the wall surface from an external source of 5000 Wm^{-2} with a step load of 10 s duration. The additional boundary conditions are:

- ambient temperature (T = 293.15 K), on the left side of the sample as in Figure 2 (a)
- perfect insulation of the top and bottom edges (no heat is transferred across these edges).

The simulated data have been added with uniform noise estimated from the IR thermal camera specification.

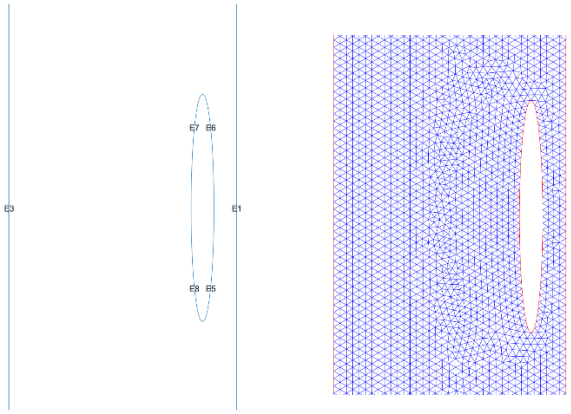

(a) (b)

Figure 2 2D FE model geometry (a) and mesh (b). IR illumination impinges from the right orthogonal to the surface

2.3 Active thermography experiment

The applicability of the soft-sensing reconstruction method has been tested to a simulacrum of a fresco painting realized in the laboratory in order to reproduce realistic defects at known positions and depths. The simulacrum has been supplied by the Laboratoire de Recherche des Monuments Historiques – LRMH (Paris, France) in the context of a collaborative EU project, LaserArt (Grant agreement ID: SMT4962062me(s), 1994-1998). It is a modern replica of a traditional fresco, realized with both material and techniques similar to that of mediaeval age, artificially aged over last 20 years. The sample is painted with colors and the surface is finished in a similar way of that of an original fresco, in such a way to present the typical emissivity of a real work of art.

Figure 3 (a) reports a scheme of the defect topology:

- bold lines represent sub-superficial defects, located between intonaco and arriccio.
- dashed lines represent in-depth defects, located between the deepest layer and the supporting concrete panel.

In this paper we focus only on disk-like defects. Results of the reconstruction will be presented as a cross section along one diameter of the disk. The reference geometry was determined after the tests by breaking the sample and measuring the fragments with a caliper; this provided a reference geometry known with less than 1 mm uncertainty. The red rectangle, in Figure 3 (a), evidences the region monitored during an active thermography test. For the sake of simplicity and without losing of generality it has been preferred focusing to only one defect in order to evidence the correct functionality of the methodology proposed. The thermogram acquired is shown in Figure 3 (b).

The active thermography test has been realised by providing the thermal load with a set of four halogen lamps and acquiring the thermograms time sequence by an Infratec–Variocam HD IR thermal camera, whose metrological specifications are reported in Table 1.

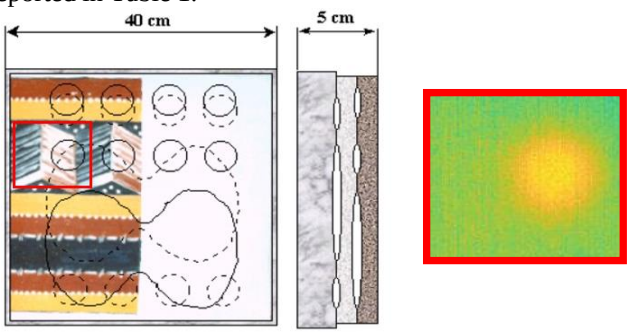

(a) (b)

Figure 3 Simulacrum defect topology with the region framed by the IR thermal camera evidenced in a red rectangle (a) and IR thermogram (b)

Table 1 IR thermal camera specifications

Sensor	Uncoated microbolometer
Spatial resolution	1024x768 pixel
Spectral range	7.5 to 14 μm
Temperature range	-40 to 1200 °C
Sensitivity	<0.05 °C
Accuracy	±1.5 °C
Frame rate	30 Hz

3. Soft-sensing reconstruction method: data pre-processing and optimization procedure

The soft-sensing method is based on an optimization process aiming to reconstruct the complete defect geometry and, as the name soft-sensing recalls, it makes use of experimental and numerical data whose difference is minimized. The experimental data are the thermograms acquired during an active thermography test and represent the infrared emission distribution on the surface of the tested sample; once emissivity is known, this can be mapped into an experimental surface temperature distribution. The numerical data are the surface temperature distribution calculated on the tested sample modelled with a FEM model able to simulate a thermography experiment. The soft-sensing algorithm, developed in Matlab, is constituted of two units: a pre-processing unit and a reconstruction one. Both the units need experimental and numerical data. The pre-processing unit has the following structure, as outlined in Figure 4:

1. first the time sequence of the thermograms measured on the tested sample during the active thermography test are loaded
2. a pre-processing of the thermograms time sequence is performed to obtain the real heat flux distribution and surface emissivity map of the tested sample, that will be used as inputs for the FE model
3. the temperature distribution of the modeled test sample is simulated by imposing a guess value for the thermal properties of the material constituting the sample itself. In this phase a region of the sample located in a sound area is considered
4. the optimization is run using as objective function the difference between the measured surface temperature of the sample and the one calculated numerically. The optimization variables are the material properties. The iteration method used for the optimization process is the steepest descent algorithm.
5. by minimizing the objective function, the material properties of the tested samples are then derived.

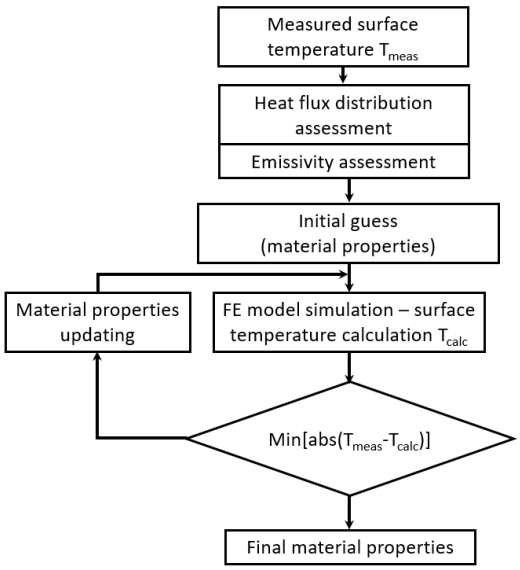

Figure 4 Pre-processing unit structure

The reconstruction unit has a structure similar to the pre-processing one, as illustrated in Figure 5:

1. at first the thermograms are loaded

2. the temperature evolution of the modeled test sample is simulated by imposing a guess for the defect geometry (shape and depth)
3. the heat flux distribution to be simulated in the FE model, the sample surface emissivity and the material properties, determined during the preprocessing, are given as inputs to the FE model
4. the optimization is then run with the same objective function and the iteration method as in the preprocessing unit. The optimization variable is the defect geometry
5. the defect geometry is iteratively reconstructed by minimizing the objective function.

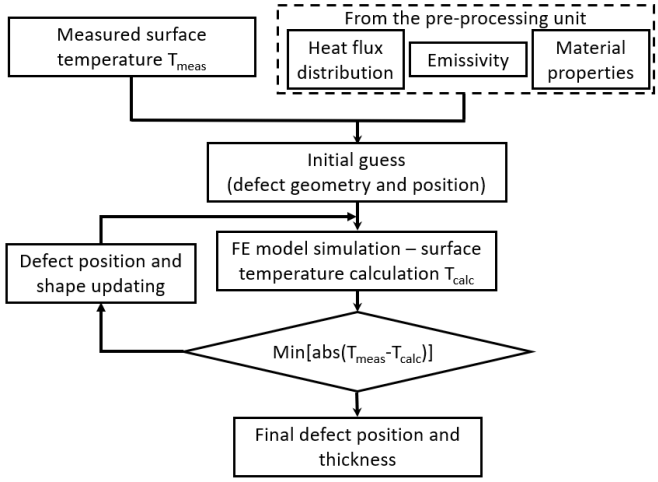

Figure 5 Reconstruction unit structure

3.1 Pre-processing procedure - Emissivity distribution and impinging heat flux profile determination

The first objective of the preprocessing is to determine the emissivity distribution of the sample surface facing the IR thermal camera and the impinging heat flux on the sample surface itself. Those data are recovered by analyzing the experimental thermogram time sequences acquired during the experiments. If a thermogram pixel is considered the time history recorded during an active thermography test will have the trend depicted by the red curve in Figure 6. When the thermal load is activated (e.g. the halogen lamps are switched on), at the time instant t_0, the temperature of the sample surface increases until the load is switched off, at the time instant t_S. From this moment on the surface temperature decreases until the thermal equilibrium is not restored.

According to the transient thermal diffusion physics, it can be assessed that when the thermal load is activated and radiates the sample surface, a small portion of the thermal flow is reflected depending on the emissivity of the surface itself while the remaining portion is absorbed by the first layer of the sample and diffused across the sample depth. Indeed, the pigmented surface materials of fresco paintings have a rather large emissivity, thus a relatively large absorption coefficient. Diffusion is commonly a much slower phenomenon than reflection. Complying with this assumption, the first thermograms in the time series acquired immediately after activating the thermal load can be considered unaffected by the sample in-depth morphology, because diffusion has not evolved yet. Those thermograms are only influenced by the very first layers (the pigments) of the sample and by the intensity and the spatial distribution of the radiated heat. The presence of an in-depth defect does not affect the spatial distribution of those thermograms. In Figure 6 the time instants considered for the emissivity and heat flux distribution assessment are evidenced by the light blue rectangle. The intial time instant is indentified with the raise time of the time history, by means of a derivative algorithm. The number of thermograms used for the emissivity and heat flow assessment is selected as a compromise between the need of averaging images affected by noise due to low emissivity and the need of catching only the superficial behaviour not affectd by the in-depth structure diffusion. In this case one thermogram was sufficient.

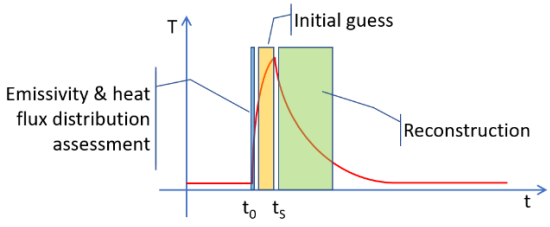

Figure 6 Sample surface temperature trend and time chunk used in the different phases of the pre-processing and reconstruction procedures

The yellow and green rectangles evidence the time instants at which thermograms will be considered for the geometry initial guess process and for the definitive reconstruction. They will be illustrated in detail in Section 3.3 and 3.4 respectively.

To demonstrate how the initial thermograms analysis can conduct to the heat flux profile and surface emissivity assessment, it can be observed the scheme in Figure 7. Picture (a) sketches a typical active thermography test on a sample whose surface is black and white striped. If the first thermogram after the thermal load activation is considered and a section along the axis x is visualised, it would have the shape of plot (b) in Figure 7. From that profile the heat flux trend and the emissivity can be recovered with the following procedure:

1. the heat flux profile is obtained by fitting the profile (b) with a symmetrical polynomial, e.g. a polynomial of degree ½ for a single radiating point source. The fitting function will be more complex if multiple radiating point sources will be used, see Figure 7 (c)
2. the emissivity surface profile is then derived as the residual or the difference between the acquired profile (b) and the fitted heat flux profile (c), which is the profile (d) in Figure 7.

In principle, emissivity could have been determined also by imaging the surface in isothermal conditions; in fact, if temperature is uniform across the surface, the infrared emission should be uniform as well. Instead, if a contrasted image is observed, this image corresponds to an uneven spatial distribution of emissivity. However, when such a method is applied at ambient temperature, the infrared signal is very low and therefore the signal to noise ratio is poor, thus producing an uncertain estimate of emissivity. The approach described in this paper instead provides an estimate of emissivity with a better signal to noise, being the surface thermally excited by the flash lamp.

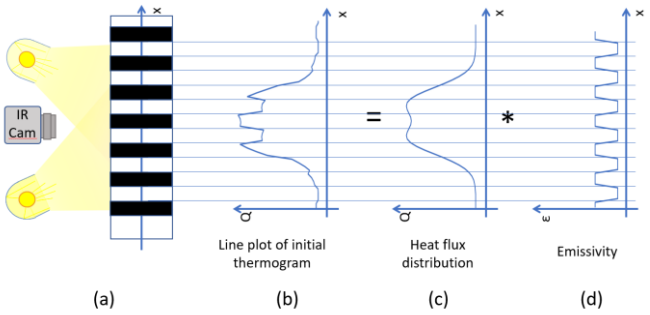

Figure 7 Heat distribution and emissivity profiles derived from the acquired one

3.2 Pre-processing procedure - Material properties determination

The FE numerical model needs as inputs the thermal and physical properties of the material composing the samples. In general, those properties are assumed to be known from the composition of the sample under test or from available technical specifications. However, when dealing with ancient artworks the composition of the samples is unknown unless tests can be performed to measure the properties of the constituent material. Unfortunately, to carry out these tests it is necessary to extract part of the material by means of coring, for example, which is a destructive intervention often impossible to carry out on artworks. Technical specifications are typically absent. Therefore, the combination of the experimental with the numerical data can be used to determine those unknown properties. The thermogram time series provided by the active thermography test are useful to evidence sound areas, for instance the portion thermogram evidenced by the blue square in Figure 8. This Region of Interest (RoI) can be selected and modeled with the FE model described in Section 2.2 considering an undamaged geometry and using as inputs the surface emissivity and the heat flux distribution profile determined in the first phase of the preprocessing (as detailed in Section 3.1. The model will be run by varying the material properties, e.g. the thermal conductivity k (in $Wm^{-1}K^{-1}$), the specific heat capacity C_p (in $Jkg^{-1}K^{-1}$) and the density ρ (in kgm^{-3}), and the temperature calculated in the region of interest in the time period corresponding to the measurement time will be exploited as input to the optimization algorithm. The latter will be based on the following problem:

$$min \sum_t \sum_x \left| T_{meas}(t,x) - T_{FEM}(t,x)|_{k,C_p,\rho} \right| \qquad (1)$$

where equation (1) is the objective function depending on the optimization variables k, C_p and ρ, T_{FEM} and T_{meas} are the surface temperatures calculated by the FE numerical model and measured during the active thermography test on the real

sample. The minimization will be performed on the average difference of the two temperature in space and time, e.g. for each pixel a RoI section whose position is given by the *x* coordinate and for all the time samples (*t*) acquired during the transient test.

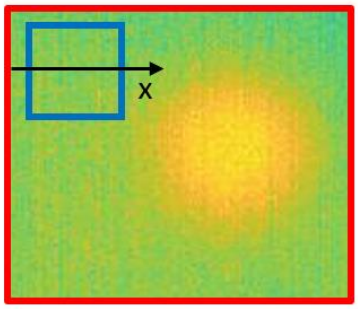

Figure 8 RoI centred on a sound area

3.3 Reconstruction procedure - Defect geometry initial guess

The reconstruction procedure starts with the assumption of an initial geometry of the defect which is estimated from the thermograms time series measured during the active thermography test. Only the time series corresponding to the heating up phase (yellow rectangle in Figure 6) will be considered because in this phase the heating flux impinging on the surface is known, in fact it has been determined during the preprocessing.

To obtain an initial estimation of the defect depth a 0D thermal wave model will be considered. The 0D model extrapolation from the physical model of sample tested is illustrated in Figure 9. The top plot of the figure represents the physical model of the sample which can be approximated by a 2D model when taking into account one sample section. The red dots in the picture represent the pixels of the thermograms acquired during the active thermography test. The 2D model can be simplified into a 1D model, conventionally adopted in PT/model correlation ([27]).

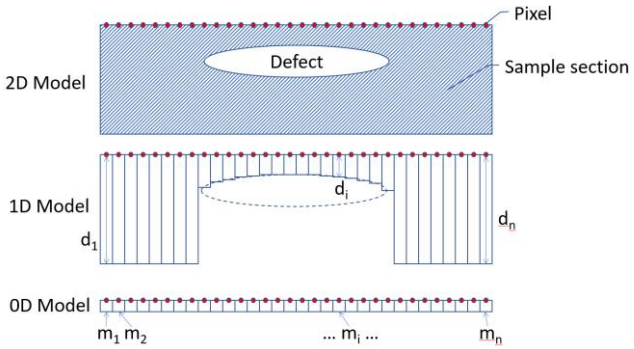

Figure 9 Relation between the physical model of the damaged samples and the corresponding 1D and 0D models

A 1D model can be seen as a series of ducts, one for each thermogram pixel, in which the thermal flow propagates, as represented in the central plot of Figure 9. Such 1D model can be further reduced to a 0D model by concentrating a given amount of mass in each pixel, as illustrated in the bottom plot of Figure 9. The mass of each pixel (m_1, m_2, …, m_i, …, m_n, if n is the number of pixels) depends on the density of the material constituting the sample and the volume of pixel, which in turn depends on the area of the pixel and the depth of the material associated to that pixel (d_1, …, d_i, …, d_n). The mass of each pixel and consequently its depth will be adjusted to fit the thermal flow measured at each pixel.

In fact, during the heating up phase at each pixel the dynamic thermal balance can be written as following:

$$Q(t) = mC_p \frac{dT(t)}{dt} \qquad (2)$$

where

$Q(t)$ is the impinging heat flux consisting on the radiant and the convective heat transfer:

$$Q(t) = Q_{rad} - h \cdot A_{pixel} \cdot (T(t) - T_{air})$$

h = convective heat transfer coefficient,

$m = \rho \cdot V_{pixel} = \rho \cdot d_{pixel} \cdot A_{pixel}$ is the mass of the material associated to each pixel,
ρ is the material density,
V_{pixel} is the volume associated to each pixel,
d_{pixel} is the depth associated to each pixel,
A_{pixel} is the area associated to each pixel as projected to the sample surface,
C_p is the specific heat capacity,
$T(t)$ is the measured temperature time history.
Equation (2) becomes:

$$m \cdot C_p \cdot \frac{\partial T(t)}{\partial t} + h \cdot A_{pixel} \cdot (T(t) - T_{air}) = Q_{rad} \qquad (3)$$

where Q_{rad} can be considered constant, because of the large temperature difference between the radiating lamp and the target surface.

Equation (3) is a first order differential equation whose solution is:

$$T(t) = \alpha \cdot \left(1 - e^{-\frac{t}{\tau}}\right) \qquad (3)$$

where α and τ respectively the asymptotic value of the temperature and the time-constant of a first order system.

The time constant of the first order system is defined as the ratio between the first order term coefficient and the zero order term coefficient:

$$\tau = \frac{m \cdot C_p}{h \cdot A_{pixel}} \qquad (4)$$

The asymptotic value can be retrieved by imposing the initial conditions at $t = 0$:

$$\begin{cases} T(0) = T_{air} \\ \frac{dT}{dt}(0) = \frac{\alpha}{\tau} \end{cases} \qquad (5)$$

Substituting those terms in equation (3) and considering $m = \rho \cdot d_{pixel} \cdot A_{pixel}$, the following equation is obtained:

$$\rho \cdot d_{pixel} \cdot A_{pixel} \cdot C_p \cdot \frac{\alpha}{\tau} + h \cdot A_{pixel} \cdot (T_{air} - T_{air}) = Q_{rad} \qquad (6)$$

from which α can be determined:

$$\alpha = \frac{\tau \cdot Q_{rad}}{\rho \cdot d_{pixel} \cdot A_{pixel} \cdot C_p} \qquad (7)$$

Figure 10 reports data acquired during a transient test as blue dots. Those data can be used to determine α and τ after a least square interpolation by an exponential function. The exponential fitting is reported in Figure 10 with the red line.

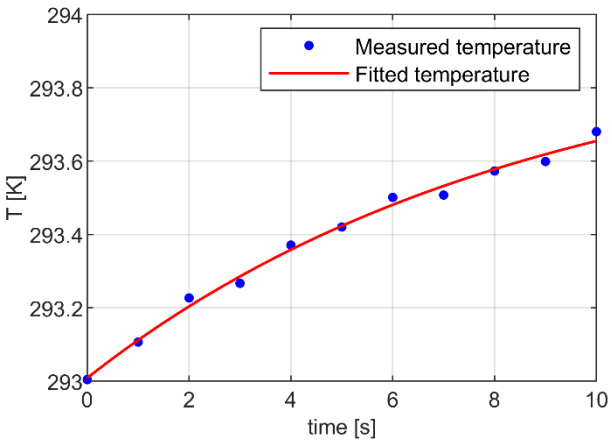

Figure 10 Measured (blue dots) and fitted (red line) time history

Once the parameters of the exponential function, α and τ are extrapolated from the measured data, the depth associated to each pixel can be determined from equation (7) as:

$$d_{pixel} = \frac{\tau \cdot Q_{rad}}{\rho \cdot C_p \cdot \alpha \cdot A_{pixel}} \qquad (8)$$

The depth calculated at each pixel will provide a rough estimation of the defect position and depth to be used as initial guess for modelling the sample with the defect. Referring to the physical model depicted in Figure 9, the depth profile recovered by applying equation (4) is shown in Figure 11 (a). The thickness of the defect cannot be determined at this stage because the 1D model assumed an open defect, as in the methods used for the determination of the back wall geometry ([27]). For modelling the complete defect geometry, it can be used a thresholding process, like it has been done in the bottom plots of Figure 11, where the threshold was set to $1/2\left(d_1 + \bar{d}\right)$, with d_1 and $\bar{d}$ as represented in Figure 11 (b) and (c). The complete geometry of the defect must be assumed then as a simple rectangle, as in Figure 11 (b), or a polygonal shape, as in Figure 11 (c).

3.4 Reconstruction procedure - Defect geometry reconstruction

The reconstruction procedure consists on an optimization process based on the experimental and numerical data, the latter obtained by running the FE model realized considering as defect geometry the one estimated by the initial guess, like the one illustrated in Figure 12. The optimization problem will be the following:

$$min \sum_{t}\sum_{x}\left|T_{meas}(t,x) - T_{FEM}(t,x)|_{x_1,\ldots,x_{n+4}}\right| \qquad (5)$$

where T_{FEM} and T_{meas} are the surface temperatures calculated by the FE numerical model and measured during the active thermography test on the real sample. In this case the optimization variables are the depth (x_1), position (x_2), width (x_3) and thickness profile, sampled at n positions, (x_4, …, x_{n+4}) of the defect which has to be determined, see Table 2 for the different defect morphologies. As evidenced in Figure 6, the experimental thermal data used in the reconstruction process are taken from the cooling down phase of the active thermography test, the green box.

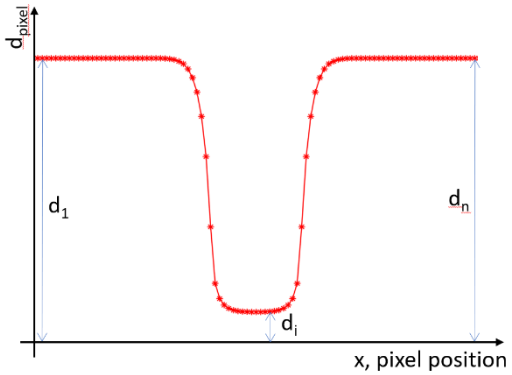

(a)

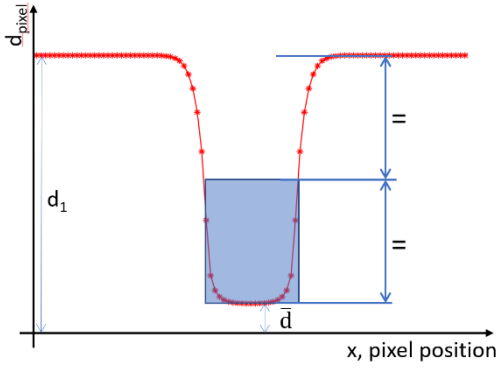

(b)

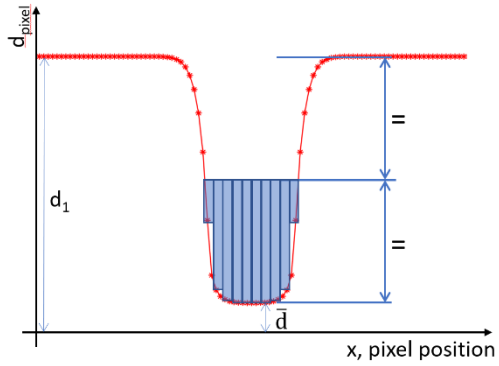

(c)

Figure 11 Defect geometry initial guess recovery from the depth profile

In order to make the calculation faster the optimization problem has been run in four steps, where the result of each step is an input for the following one. At each step a simple modification of the defect geometry is brought as sketched in Table 3:
Step 1: rigid displacement of the initial guess shape in x and y-direction
Step 2: rigid displacement of the defect shape obtained in Step 1 in x-direction and defect resizing
Step 3: rigid displacement of the defect shape obtained in Step 2 in y-direction
Step 4: reshaping of the defect obtained in Step 3, by varying its thickness th_i.

The benefit obtained by dividing the optimization process into the aforementioned four steps is evidenced by the convergence plot of the objective function reported in equation (5), that is shown in Figure 13.

Table 2 Defect morphology

Shape function	x_1	x_2	x_3	x_i i=4:n+4	Plot
Rectangle	Depth	Position	Width	Thickness	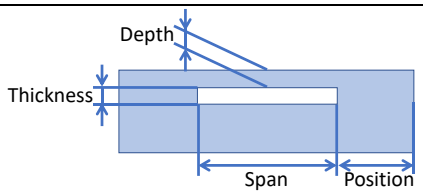
Ellipse	Depth	Position	Width (major axis)	Thickness (minor axis)	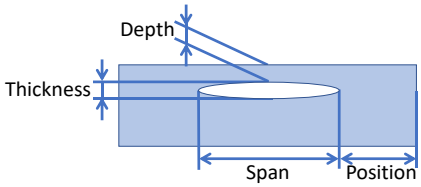
Polynomial	Depth	Position	Width	th_j j=1:n	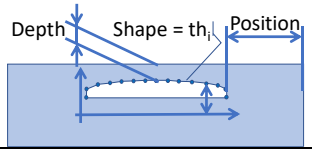

Table 3 Optimisation steps

Steps	Defect shape update
Step 1	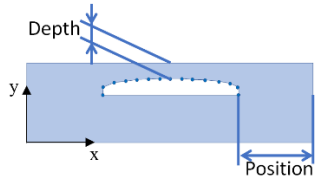
Step 2	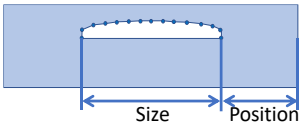

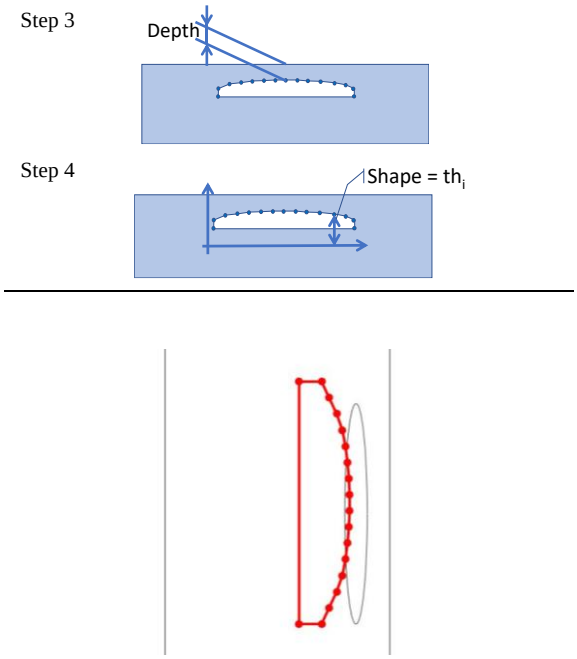

Figure 12 FE model geometry (grey) with the defect initial guess (red)

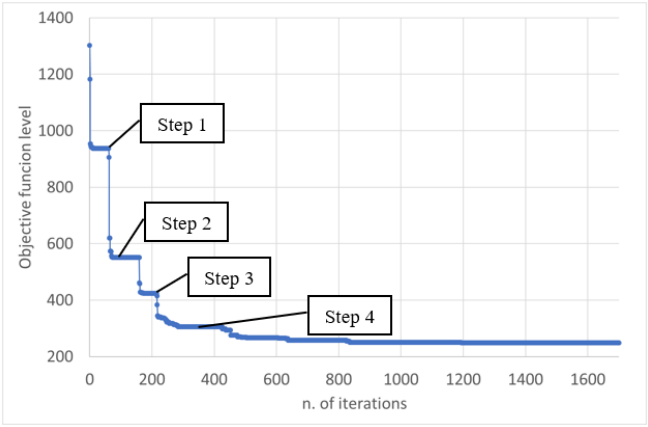

Figure 13 Objective function convergency plot

4. Discussion of results

The soft-sensing reconstruction procedure has been tested first on data provided by a virtual experiment based on the same FE model used to produce the numerical data provided as input to the optimization problem and then on experimental data measured on the fresco simulacrum described in Section 2.3. The results of the reconstruction are illustrated in Section 4.1 and 4.3 for the virtual and real test respectively.

4.1 Soft-sensing reconstruction method applied to the virtual experiment

The virtual experiment consists in the running of the FE model described in Section 2.2 to provide the temperature profile occurring on the modelled sample surface when the active thermography test is simulated. The geometry of the sample includes a defect with dimensions and depth reported in Section 2.2. This process, also called forward calculation, is the simulation of the experiment and provides the surface temperature profile evolution during the testing time as shown in Figure 14. For this simulation the maximum over-heating is 20 K. Those temperature data will be exploited (as if they were experimental data) first to estimate the initial guess defect geometry and then as reference data to be given in input to the optimization problem.

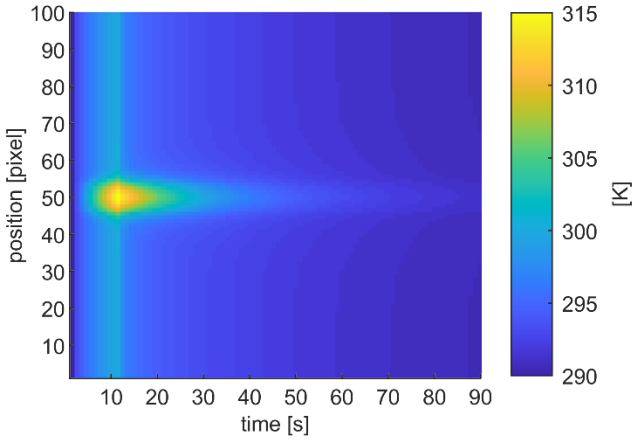

Figure 14 Simulated temperature profile evolution in time

The results of the reconstruction process are shown in Figure 15. The sample geometry with the simulated defect is drawn in grey. The initial guess geometry estimated with the procedure described in Section 3.3 starting from the surface temperature profile shown in Figure 14 is the green line. At this point the FE model will be updated using as defect geometry the initial guess and the optimisation process will start by minimising the real temperature profile (Figure 14) with the one simulated at the different optimisation steps, as described in Table 3. Figure 15 reports the defect geometry reconstructed at Step 4 and at the end of the complete optimisation process. Those geometries are in blue and red, respectively.

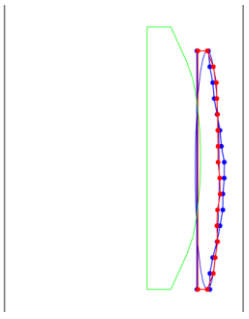

Figure 15 Reconstructed defect geometry (grey: real geometry, green: initial guess defect geometry, blue: reconstructed defect geometry at Step 4, red: reconstructed defect geometry at the end of the optimisation process)

Observing the optimization result it can be concluded that the defect depth, width and thickness have been determined

with good accuracy, nevertheless there is a slight deviation in the profile curvature which can be related to the lateral thermal diffusion at the edge of the defect. The diffusion flow (represented by the red arrows) is depicted in Figure 16 for the real configuration (on the left) and for the reconstructed one (on the right). The dashed line in the left part of the figure represents the real shape of the defect, to evidence the curvature mismatch. The discrepancy between the real and reconstructed defect profile is ascribed to the following reasons:

- the initial guess defect shape has been forced arbitrarily to have the shape of the green curve in Figure 15, as described in Section 3.3
- the optimization algorithm uses as reference in the objective function the temperature on the sample surface. From the surface point of view, what is behind the defect is hidden by the defect itself in terms of thermal diffusion. This is not true anymore only at the edge of the defect and the algorithm "compensates" this effect with a change in defect curvature.

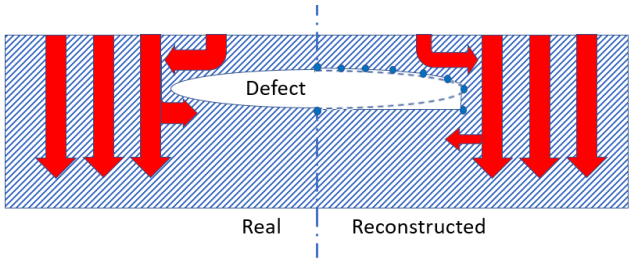

Figure 16 Lateral thermal flow in the real (left) and reconstructed (right) configuration

4.2 Soft-sensing reconstruction method uncertainty assessment

The quantity to be measured by the procedure proposed is the position of the defect profile inside the sample tested, which is obtained indirectly by the soft-sensor from a temperature distribution measurement. Therefore, the uncertainty of the method can be given in terms of geometric inaccuracy, i.e. in the reconstruction of the defect profile and in terms of recomputed temperature distribution on the sample surface.

The discrepancy between the reconstructed profiles and the original one (grey line in Figure 15) is plotted in Figure 17. It has been computed as the absolute error between the actual and the reconstructed defect abscissa. The calculation has been limited to the convex portion of the geometry. The maximum error occurs when considering the profile reconstructed with the initial guess (green line); the maximum error is 180% of the defect thickness. If the optimisation is stopped at step 1 (blue line) the maximum error drops to 20%, while if the optimisation is run until total convergence the maximum error goes below the 5% of the defect thickness.

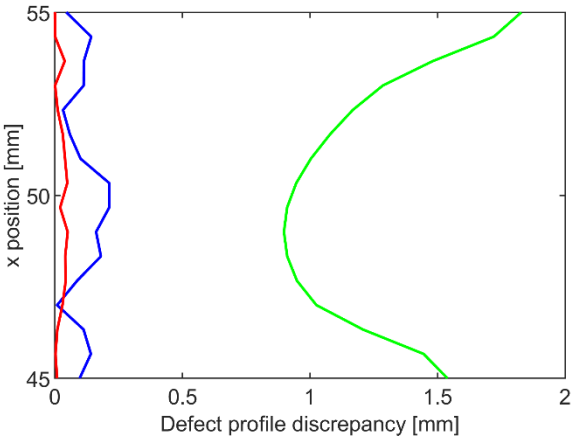

Figure 17 Geometric discrepancy between the reconstructed profiles and the original one (green line: initial guess, blue line: step 1 optimisation, red line: final optimisation)

The accuracy of the reconstruction can be measured also by recomputing the surface thermal profile with the FE model using as defect geometry the one obtained with the optimisation process. The difference between the calculated thermal profile and the real one (e.g. the one plotted in Figure 14) is shown in Figure 18. The maximum temperature difference is of 1.6 K. If 1.6 K error is produced by a 5% geometric discrepancy, one can calculate the geometric error caused by the typical inaccuracy of the sensor used to measure the thermogram series, which is 1.5 K, as reported in Table 1. Considering a linear correspondence between defect position and surface temperature, the geometric uncertainty associated to the sensor accuracy is 4.7%. The total uncertainty is the combination of the uncertainty related to the temperature measurement (4.7%) and the one related to the indirect procedure (5%) thus resulting in a combined uncertainty up to about 7 % of the defect thickness.

If the same thermal difference is calculated by using in the FE model the initial guess defect geometry, as would happen if only the experimental data would be used to fit the 0D model and the optimisation process would not been run, the maximum temperature difference is 8 K, see Figure 19.

If instead it is considered an open defect, the blue line in Figure 20, like occurs in literature ([20], [27]), the maximum difference is 1.2 K but spread over a biggest area and a longer duration in time, see Figure 21.

Finally, it has been assessed the error on the reconstruction results depending on an error in the heat flux distribution estimated during the preprocessing. By running the reconstruction algorithm with a heat flux underestimated of the 10%, the reconstructed geometry presents an overestimation of the 9.3% in the width of the defect.

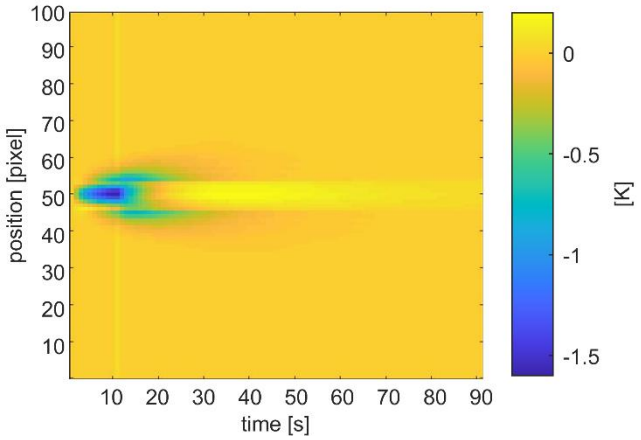

Figure 18 Difference between the real surface thermal distribution and the calculated one using the reconstructed defect geometry

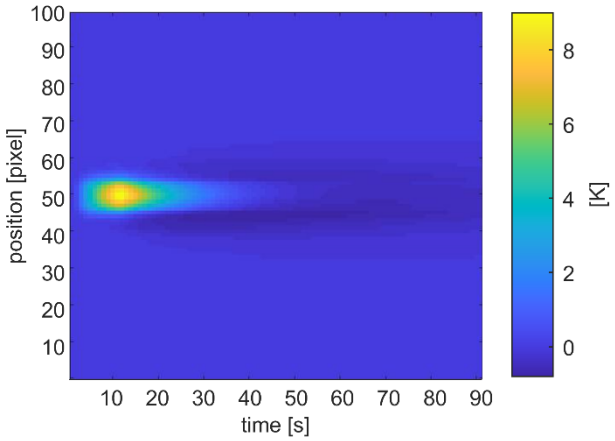

Figure 19 Difference between the real surface thermal distribution and the calculated one using the initial guess defect geometry

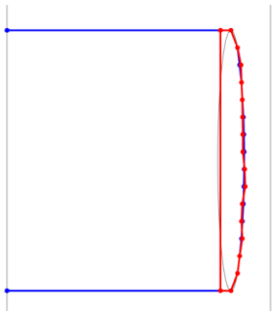

Figure 20 Reconstructed defect geometry (red: reconstructed defect geometry at the end of the optimisation process, blue: reconstructed defect geometry considering an open defect)

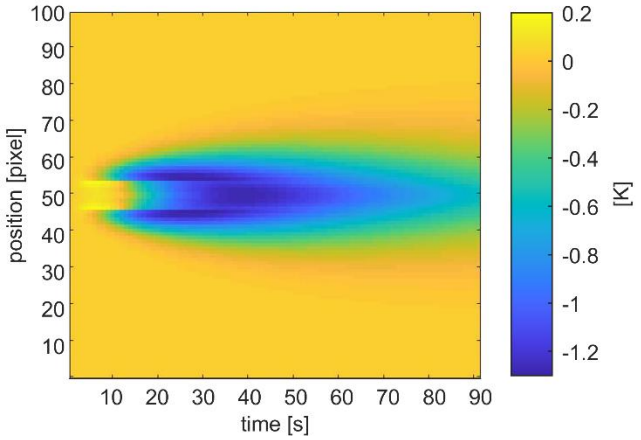

Figure 21 Difference between the real surface thermal distribution and the calculated one using an open defect geometry

4.3 Soft-sensing reconstruction method applied to the active thermography experiment

This section presents the reconstruction results obtained from the real active thermography test described in Section 2.3. The RoI chosen for the defect reconstruction process is shown in Figure 22; the section considered for the calculation is the x axis.

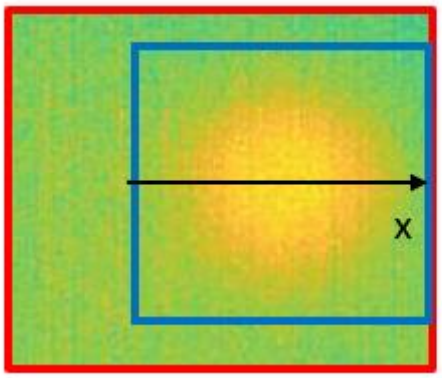

Figure 22 Thermogram (red rectangle) centred on a defected area: the blue square represents the RoI analysed and the x-axis the diameter along which the reconstructed defect profile will be plotted

The measured temperature distribution along the x-axis and its evolution in time is shown in Figure 23. With respect to the simulated data the measured ones are more affected by the noise. This is due to the fact that the thermal load imposed to the real structure was much less powerful with respect to the simulated one to avoid structure distortions or additional damages. In fact, in the experimental validation the maximum over-heating is 2 K, in order to reduce thermal stresses on the structure.

The results of the reconstruction process are shown first in terms of convergency plot which is similar to the one obtained in the virtual experiment; compare Figure 13 and Figure 24.

Both plots evidence the 4 steps of the optimisation process; they are very similar except for the presence of some instabilities in the convergence related to experimental data. This effect is due to the presence of noise on the experimental data used as a reference in the optimization problem.

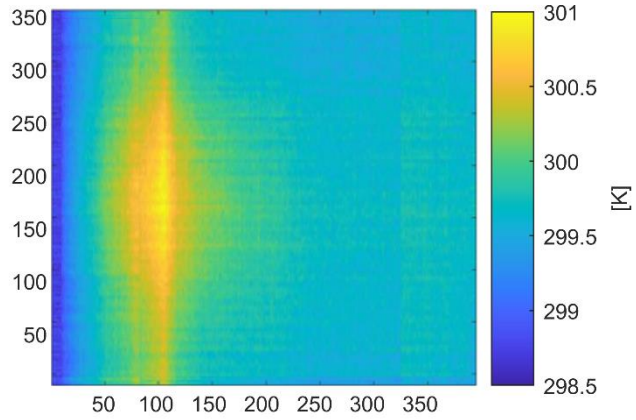

Figure 23 Measured temperature profile evolution in time

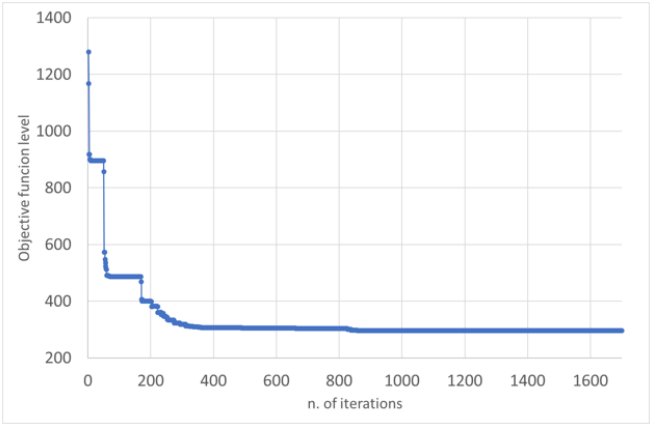

Figure 24 Objective function convergency plot for the experimental test

The reconstructed defect geometry is plotted in Figure 25 in red, together with the initial guess (green line).

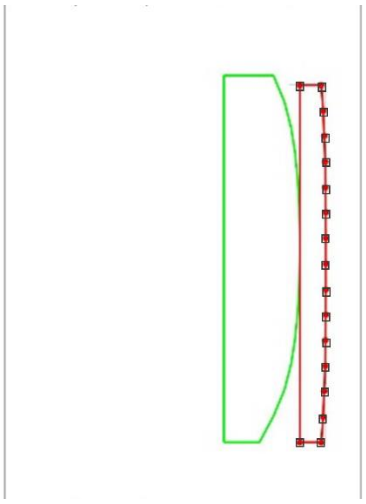

Figure 25 Reconstructed defect geometry (green: initial guess defect geometry, red: reconstructed defect geometry, the grey squares are the reference geometry)

With respect to the real expected defect geometry (grey squares) the reconstructed one underestimates the thickness of the defect and presents the curvature mismatch due to the border effect as explained in Section 4.1. The depth and the width of the defect are accurately reconstructed. The underestimation of the thickness can still be ascribed to the noise affecting the experimental data.

5. Conclusion

In this paper, the authors presented a soft-sensing procedure for artworks inner defect reconstruction based on the correlation between experimental and numerical data. The first are the temperature distribution on the surface of the object under test and its evolution on time obtained by performing an active thermography test. The numerical data are provided by a FE model of the tested sample considering an initial guess of the unknown defect geometry and iteratively varied until the difference between the surface temperature calculated and the measured one is minimized. In fact, it is possible to update the model with the measured data (infrared images) and change the geometry of the simulated inner defect, until the surface temperature distribution calculated matches the measured one.

The procedure has been firstly applied to thermograms simulated numerically with the same FE model used in the optimization problem in order to test the reconstruction accuracy. It has been evidenced that the defect geometry was precisely recovered in terms of depth, width and thickness. Uncertainty in reconstructed defect geometry accounts for about 7 % of defect thickness, obtained by combining the uncertainty of the numerical reconstruction method to the uncertainty of the infrared camera. A slight mismatch occurs only on the defect shape curvature influenced by the thermal lateral diffusion arising at the edge of the defect.

For the purpose of validating the soft sensing method, measurements have been performed on a real fresco with defects artificially created, having known geometry and position. In particular, a modern replica of a traditional fresco, realized with both material and techniques similar to that of mediaeval age, artificially aged over last 20 years, has been used. The application of the soft-sensing reconstruction procedure to real data provided by an active thermography test on the simulated ancient fresco confirmed the effectiveness of the method also when coping with noisy data. The inner known delamination has been reconstructed with the same level of uncertainty achieved in the numerical simulation.

Acknowledgements

Authors would like to acknowledge the contribution of Dr. Giuseppe Pandarese for the support in experimental tests.

References

[1] Grys S 2012 New thermal contrast definition for defect characterization by active thermography *Measurement* **45(7)** 1885

[2] Ruizhen Y and Yunze H 2016 Optically and Non-optically Excited Thermography for Composites: A review *Infrared Physics & Technology* **75** 26

[3] Ciampa F, Mahmoodi P, Pinto F and Meo M, 2018 Recent Advances in Active Infrared Thermography for Non-Destructive Testing of Aerospace Components *Sensors* **18** 609

[4] Montanini R and Freni F 2012 Non-destructive evaluation of thick glass fibre-reinforced composites by means of optically excited lock-in thermography *Composites: Part A – Applied Science and Manufacturing* **43(11)** 2075

[5] Berger D, Brabandt D, Bakir C, Hornung T, Lanza G, Summa J, Schwarz M, Herrmann HG, Pohl M and Stommel M 2017 Effects of defects in series production of hybrid CFRP lightweight components – detection and evaluation of quality critical characteristics *Measurement* **95** 389

[6] Hellstein P and Szwedo M 2016 3D thermography in non-destructive testing of composite structures *Measurement Science and Technology* **27(12)**

[7] Avdelidis N P and Moropoulou A 2004 Applications of infrared thermography for the investigation of historic structures *Journal of Cultural Heritage* **5(1)** 119

[8] Castellini P, Martarelli M, Lenci S, Quagliarini E, Silani M and Martellone A 2017 Diagnostic survey on frescoes paintings in Pompei by active IR-thermography *IMEKO International Conference on Metrology for Archaeology and Cultural Heritage, MetroArchaeo* 51

[9] Meola C, Carlomagno G M, Squillace A and Giorleo G 2002 Non-destructive control of industrial materials by means of lock-in thermography *Measurement Science and Technology* **13(10)**

[10] Wang F, Wang Y, Liu Y and Wang Y 2018 Theoretical and experimental study on carbon/epoxy facings-aluminium honeycomb sandwich structure using lock-in thermography, *Measurement* **126** 110

[11] Montanini R 2010 Quantitative determination of subsurface defects in a reference specimen made of Plexiglas by means of lock-in and pulse phase infrared thermography *INFRARED PHYSICS & TECHNOLOGY* **53(5)** 363

[12] Krapez J C, Boscher D, Delpech P, Déom A, Gardette G and Balageas D 1992 Time-Resolved Pulsed Stimulated Infrared Thermography Applied to Carbon-Epoxy Non-Destructive Evaluation *QIRT '92, France*

[13] Pawar S S and Peters K 2013 Through-the-thickness identification of impact damage in composite laminates through pulsed phase thermography *Measurement Science and Technology* **24(11)**

[14] Ólafsson G, Tighe R C and Dulieu-Barton J M 2018 Improving the probing depth of thermographic inspections of polymer composite materials *Measurement Science and Technology* **30(2)**

[15] Liu Y, Wu J Y, Liu K, Wen H L, Yao Y, Sfarra S and Zhao C 2019 Independent component thermography for non-destructive testing of defects in polymer composites *Measurement Science and Technology* **30(4)**

[16] Liu K, Li Y, Yang J, Liu Y and Yao Y 2020 Generative Principal Component Thermography for Enhanced Defect Detection and Analysis *IEEE Transactions on Instrumentation and Measurement* **1-1**

[17] Liu Y, Liu K, Yang J and Yao Y 2020 Spatial-Neighborhood Manifold Learning for Nondestructive Testing of Defects in Polymer Composites *IEEE Transactions on Industrial Informatics* **16(7)** 4639

[18] Theodorakeas P and Koui M 2018 Depth Retrieval Procedures in Pulsed Thermography: Remarks in Time and Frequency Domain Analyses *Applied Sciences* **8** 409

[19] Sharath D, Menaka M and Venkatraman B 2013 Effect of defect size on defect depth quantification in pulsed thermography *Measurement Science and Technology* **24(12)**

[20] Lugin S and Netzelmann U 2007 A defect shape reconstruction algorithm for pulsed thermography *NDT & E International* **40(3)** 220

[21] Elhassnaoui A, El Ballouti A and Sahnoun S 2013 Reconstruction of a triangular geometry defects in inaccessible face by a model of active thermography *Journal of Optoelectronics and Advanced Materials* **15**

[22] Elhassnaoui A and Sahnoun S 2014 A three-dimensional reconstruction algorithm for pulsed thermography *Journal of Material Environmental Sciences* **5(4)** 983

[23] Di Maio R, Mancini C, Meola C and Piegari E 2012 Numerical modelling of architectonic structures' thermal response. Laboratory and in-situ data analysis *11th QIRT conference, Italy*

[24] Di Maio R, Maierhofer C, Mancini C and Piegari E 2013 A quantitative analysis of IRT data for the evaluation of plaster degradation at the Dome of Magdeburg (Germany) *EGU General Assembly 2013, Austria*

[25] Zhao Y, Mehnen J, Sirikham A and Roy R 2017 A novel defect depth measurement method based on Nonlinear System Identification for pulsed thermographic inspection *Mechanical Systems and Signal Processing* **85** 382

[26] Marchuzzi F and Marinetti S 2008 Efficient reconstruction of corrosion profiles by infrared thermography *4th AIP International Conference and the 1st Congress of the IPIA*, Journal of Physics: Conference Series 124

[27] Riechter R, Maierhofer C and Kreutzbruck M 2013 Numerical method of active thermography for the reconstruction of back wall geometry *NDT&E International* **54** 189

[28] Fortuna L, Graziani S, Rizzo A and Xibilia M G Soft Sensors for Monitoring and Control of Industrial Processes 2007 Springer-Verlag New York

[29] Souza F A A, Araújo R and Mendes J 2016 Review of soft sensor methods for regression applications *Chemometrics and Intelligent Laboratory Systems* **152** 69

[30] Castellini P, Paone N and Tomasini E P 1996 The laser Doppler vibrometer as an instrument for non-intrusive diagnostic of works of art: application to fresco paintings *Optics & Lasers in Engineering* **25** 227

[31] Castellini P, Esposito E, Paone N and Tomasini E P 2000 Non-invasive measurements of damage of frescoes paintings and icon by laser scanning vibrometer: Experimental results on artificial samples and real works of art *Measurement: Journal of the International Measurement Confederation* **28(1)** 33

[32] Castellini P, Esposito E, Legoux V, Paone N, Stefanaggi M and Tomasini E P 2000 On-field validation of non-invasive Laser

Scanning Vibrometer Measurement of damaged frescoes: experiments on large walls artificially aged *Journal of Cultural Heritage* **21(1)** S349
[33] Collini L, Garziera R and Mangiavacca F 2011 Development, experimental validation and tuning of a contact-less technique for the health monitoring of antique frescoes *NDT and E International* **44(2)** 152
[34] Tornari V 2007 Laser interference-based techniques and applications in structural inspection of works of art *Analytical and Bioanalytical Chemistry* **387(3)** 761
[35] Tornari V, Bonarou A, Zafiropulos V, Fotakis C, Doulgeridis M, 2000 Holographic applications in evaluation of defect and cleaning procedures *Journal of Cultural Heritage* **1(2)** S325
[36] Castellini P, Abaskin V and Achimova E 2008 Portable electronic speckle interferometry device for the damages measurements in veneered wood artworks *Journal of Cultural Heritage* **9(3)** 225
[37] Tornari V, Bonarou A, Castellini P, Esposito E, Osten W, Kalms M, Smyrnakis N and Stasinopulos S 2001 Laser based systems for the structural diagnostic of artworks: An application to XVII century Byzantine icons *Proceedings of SPIE - The International Society for Optical Engineering* 4402 172
[38] Groves R M, Pradarutti B, Kouloumpi E and Osten W 2009 2D and 3D non-destructive evaluation of a wooden panel painting using shearography and terahertz imaging *NDT and E International* **42(6)** 543
[39] Calicchia P, De Simone S, Di Marcoberardino L and Verardi P 2018 Exploring the potential of a frequency resolved acoustic imaging technique in panel painting diagnostics *Measurement* **118** 320
[40] Meola C and Carlomagno G M 2004 Recent advances in the use of infrared thermography *Measurement Science and Technology* **15(9)**